Received: 24 June 2023 | Revised: 7 October 2023 | Accepted: 12 October 2023

DOI: 10.1111/jace.19532

Journal of the American Ceramic Society

RESEARCH ARTICLE

Flash sintering of tungsten at room temperature (without a furnace) in <1 min by injection of electrical currents at different rates

Emmanuel Bamidele | **Syed I. A. Jalali** | **Alan W. Weimer** | **Rishi Raj**

Materials Science Engineering Program, University of Colorado Boulder, Boulder, Colorado, USA

Correspondence
Rishi Raj, Materials Science Engineering Program, University of Colorado Boulder, Boulder, CO 80309, USA.
Email: rishi.raj@colorado.edu

Funding information
NASA, ESI Program, Grant/Award Number: 80NSSC21K0225; Ames Research Center, Grant/Award Number: 0NSSC21K0225; Office of Naval Research, Grant/Award Number: N00014-18-1-2270

Abstract

Sintering of tungsten nominally requires several hours at ultrahigh temperatures. We show this refractory metal can be sintered quickly by direct injection of current into dog bone shaped specimens. The current rate was varied from 10 A s^{-1} (fast) to 0.1 A s^{-1} (slow), leading to sintering in 2–200 s, respectively. Sintering occurred at the same current density, regardless of the current rate. In all instances, the samples sintered when they reached 1000°C. The phenomenological behavior of flash sintering of metals is described by three stages: an incubation time followed by electroluminescence, and finally by abrupt sintering to full density. It is conjectured that rapid sintering is instigated by the formation of Frenkel pairs (vacancies and interstitials), as well as electrons and holes. The point defects accelerate mass transport, whereas electrons and holes recombine to form photons. Calorimetric measurements show an endothermic reaction attributed to the creation of defects. Estimates suggest an unusually large concentration of Frenkel pairs. PS: Flash sintering is different than electro-discharge-sintering where a capacitor is discharged in a few milliseconds to sinter a metal. Here, instead of dumping large amount of energy at once, a power supply is programed to control the rate of current injection.

KEYWORDS
current rate sintering, flash sintering, refractory metals, tungsten sintering

1 | INTRODUCTION

The interest in field-assisted sintering of materials started several decades ago with microwave sintering.[1] A major boost was the advent of spark plasma sintering (SPS).[2] SPS has evolved as an enabling technology for densifying metals and ceramics that are normally difficult to consolidate.[3] This field received a further boost in the discovery of flash sintering where dog bone samples could be sintered without graphite dies in open air, within a conventional furnace below 1000°C, by applying field and current directly to the specimen.[4]

Flash sintering has been shown to apply widely[5]; to nearly all oxides as well as non-oxide ceramics.[6] The history of flash has been published recently[5]; it gives an overview of the developments since 2010. A recent review by Yu et al.[7] is also insightful. Two other advanced processing methods, ultrafast heating rate,[8] and cold sintering,[9] have emerged. Interestingly, the equivalence between ultrafast heating rate experiments and flash sintering was

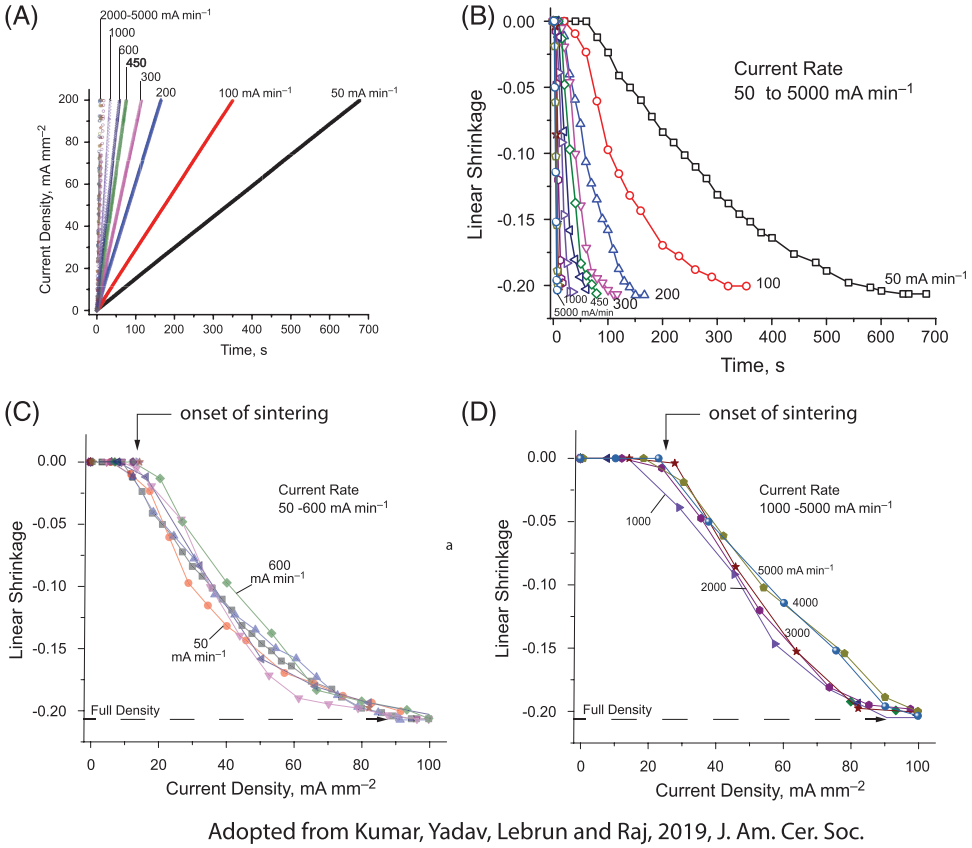

Adopted from Kumar, Yadav, Lebrun and Raj, 2019, J. Am. Cer. Soc.

FIGURE 1 (A) Flash sintering of yttrium stabilized zirconia with current rates ranging over two orders of magnitude. (B) Sintering strain as a function of time. (C and D) Sintering as a function of the current density showing that sintering depends solely on the current density not on the rate at which it is injected.

recently demonstrated in experiments with thin layers made from fine powders could be heated at a rapid rate with a propane torch.[10]

The design of flash experiments enables open access to the specimens. In this way, in-operando measurements are enabled: Sintering is measured with a rapid-rate camera,[4] the temperature with a pyrometer,[11] and the optical emission spectrum with a spectrometer.[12]

It has been possible to perform in situ calorimetric measurements during flash by comparing the input electrical power with the energy expended in radiation and convection, and the energy stored as specific heat. The deficit implies an endothermic reaction, which is attributed to the formation of defects.[13]

The sintering of metals embodies a uniquely simplifying feature: The experiment can be carried out at room temperature, without a furnace, using current injection to raise the specimen temperature until it flashes and sinters. We present experiments on tungsten powders, with and without a furnace, to assess the influence of furnace heating on the sintering behavior.

Current rate flash sintering was first carried out with yttria-stabilized zirconia (YSZ). Those results are summarized in Figure 1. They give the unusual result that the extent of sintering depends only on the instantaneous value of the current density, despite the rate of current having been increased by two orders of magnitude.[14] We show that flash sintering of tungsten exhibits similar behavior.

The objective of the present work is to differentiate between flash sintering in ceramics and metals.[14] We show that sintering of metals can be separated into three regimes: An incubation period that is followed by the onset of electroluminescence, and finally by abrupt sintering to full density. *The principal difference is that in ceramics, sintering occurs continuously as the current is increased, while in metals, it occurs abruptly at a specific current density*.

It is possible that flash sintering of metals is equivalent to electro-discharge-sintering, also called electric-discharge-capacitance, capacitor-discharge-sintering, electric-pulse-sintering, and so on,[15] where a large amount of energy stored in a capacitor is dumped within a few milliseconds into a powder-pressed sample of a metal, causing it to sinter. Nevertheless, the ability to understand how current rate can be controlled for time dependent sintering can advance the science of flash. It may also have technological significance: for example, it can be applied

to additive manufacturing where small quanta of metal can be sequentially sintered with electrical current for building ready-to-use metal parts.

2 | METHODS

Tungsten powder with a particle size of 12 μm was purchased from Alfa Aesar. The powder was cold pressed into dog bone shapes. The specimens for furnace-ON experiments had a gage length of 16 mm, width of 3.5 mm, and a thickness of 1.45–1.5 mm. Specimens for the furnace-OFF experiment had a gage length of 20 mm, were 3.3–3.5 mm wide, and were 0.55–0.65 mm thick. The powders were pressed without a binder, as the presence of the binder hindered sintering under flash. The pressure of 172–200 MPa under a Carver hydraulic press was deployed. The green density of these samples, measured by the Archimedes method, ranged from 77% to 80%.

Electrical current to the specimens was supplied by a KEPCO KLN30-100 Power Supply rated for 30 V and 100 A. Small holes, 1.1 mm in diameter, were drilled into the ears of the dog bones. Tungsten wire threaded through these holes served as the electrodes. The flash experiments were done in a glove box, the Genesis model, manufactured by Vacuum Atmosphere Company, USA. Argon gas (99.9% purity) was procured from Airgas, USA. The oxygen level in the Glovebox was 20 ppm.

The in-operando resistance was determined from the voltage measured at two inner electrodes just inside the current electrodes, by the so-called four point method. The ratio of this voltage and the current injected through the outer electrodes was plotted as an *I*–*V* curve, the slope of which gave the resistance in Ω. Multiplying by the cross section of the specimen and dividing by the gage length between the inner electrodes yielded the specific resistivity of the metal in units of Ω cm.

Two types of experiments were performed, one with furnace heating and the other without. In the case of furnace-ON experiments, the temperature was set at 800°C.

The specimen was imaged in real time with a CCD camera manufactured by Imaging Source at a rate of 10 frames per second. The optical emission spectrum was measured with a spectrometer (USB4000-UV-VIS) manufactured by Ocean Optics. The spectrometer was focused on the specimen; a collimating lens connected to an optical fiber was interface with the Ocean Optics hardware and was read into the computer.

The specimen temperature was measured with a CTLM-1HCF4-C3 pyrometer manufactured by Micro-Epsilon (CT-SF22-C8). The emissivity was set at 0.35.[16] The data collected from the pyrometer were converted to temperature using our data acquisition software. The pyrometer readings were calibrated against the furnace temperature with a dummy specimen for different values of the emissivity, from 0.25 to 0.35. They gave a 50°C range for the difference between the furnace temperature measured with a thermocouple and the pyrometer reading for this range of emissivities. Thus, the data presented below may contain an error bar of 50°C.

Home built software[14] was used to control the rate of current injection (which was varied from 0.1 to 10 A s^{-1}). The data were interfaced to the computer software with a National Instrument Data Acquisition card. The current from the power source was recorded as a function of time.

The sintering strain (contraction) was measured from images acquired with the CCD camera, using the Fiji, an ImageJ software. The shrinkage, ε was obtained from

$$\varepsilon = \ln\left(\frac{L}{L_o}\right) \tag{1}$$

where L is the length measured as a function of time during sintering, L_o, the initial length is set equal to the holes drilled to carry the current from the electrodes.

The volumetric shrinkage, ϵ_a, which is related to the green density, ρ_g, and the time-dependent density, ρ, is described by[17]

$$\epsilon_a = 3\epsilon = \ln\left(\frac{\rho_g}{\rho}\right) \tag{2}$$

The theoretical density of tungsten was set equal to, 19.3 g cm^{-3}.

3 | RESULTS

The results are presented in terms of the current density, or time. They are equivalent parameters as the current rate was held constant. Five current rates ranging from 0.1 to 10 A s^{-1} were employed. Sintering occurred at about 200 s at 0.1 A s^{-1}, and in just 2 s at 10 A s^{-1}.

Several results are presented: (i) sintering as a function of time, and current density, (ii) the change in resistance, (iii) the change in temperature with time as the specimen flashes and sinters, and (iv) the estimate of the endothermic enthalpy calculated from the difference between the input electrical energy and the energy dissipated by radiation and convection and stored as specific heat.

After the first sintering cycle, Cycle 1, the specimen becomes a dense polycrystal. The flash cycle was repeated twice on this specimen, called Cycles 2 and 3. The flash in powders involves an abrupt removal of particle–particle interface resistance, which is not present in Cycles

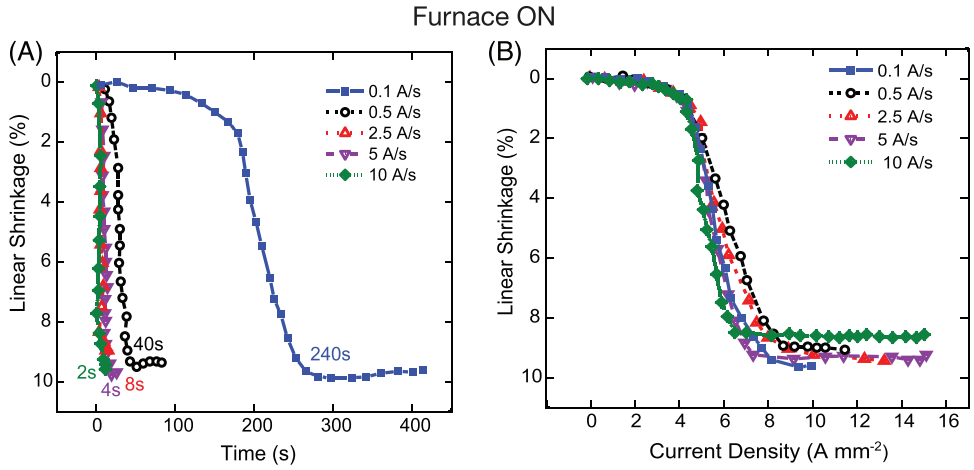

FIGURE 2 Experiments with furnace-ON: (A) linear shrinkage measured as a function of time while the current is increased at constant rates, ranging from 0.1 to 10 A s^{-1}; (B) when the strain is plotted against the current density then the data for all current rates merge into an overlapping curve, suggesting current density as the fundamental sintering parameter.

2 and 3. These latter cycles were highly reproducible pointing toward removal of defects when the current is turned off, and reintroduction of defects when the cycle is repeated. It is these cycles with dense specimens that are used to draw conclusions about the nature of the flash behavior.

3.1 | Sintering

We measured the linear strain according to Equation (1), which can be translated into relative density with Equation (2), using the green density to be approximately $\rho_g \approx 0.77$. The results for experiments carried out at current rates ranging from 0.1 to 10 A s^{-1} are shown in Figure 1. The maximum sintering strain is approximately 8.0%–8.5%. The application of Equation (2) then yields finish density of 98%–100%. The Archimedes density was measured to be 98%.

The sintering data from furnace-ON experiments are given in Figure 2. All samples sintered to full density, as is evident from the saturation of the sintering strain. The time for sintering was as short at 2 s at 10 A s^{-1}, lengthening to about 250 s at 0.1 A s^{-1}. Full sintering was achieved at a current density of 6—8 A mm^{-2}. The coalescence of the data when plotted against the current density shows that densification is independent of the current rate, and that the current density is the key parameter in flash sintering. This result is similar to the behavior in 3YSZ presented in Figure 1 with one difference. In the case of the ceramic, densification occurred continuously with current, whereas, here, all densification takes place abruptly at a certain value of the current density.

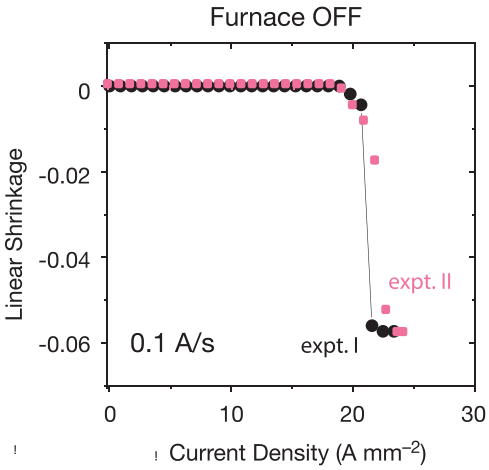

FIGURE 3 Experiments with furnace-OFF. Shrinkage as a function of the current density at a current rate of 0.1 A s^{-1}, without furnace heating.

A similar behavior is seen in the furnace-OFF experiment, carried out at 0.1 A s^{-1}, given in Figure 3. The experiment was repeated twice to check reproducibility. The difference between the furnace-OFF and furnace-ON experiments is the current density for the onset of sintering, which is 20 A mm^{-2} without, and 6—8 A mm^{-2} with the furnace. The higher current density for the furnace-OFF case means that both the temperature of the specimen and the current density play a role. The furnace temperature of 800°C partly compensates for the Joule heating provided by the current density, that is, less current is needed to reach the desired temperature for the onset of sintering. The role of temperature is discussed in Section 3.3.

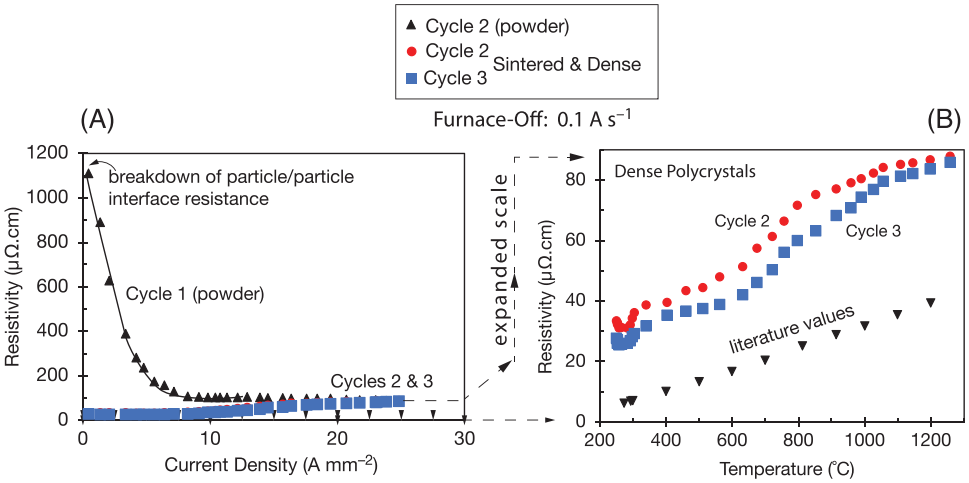

FIGURE 4 The change in resistivity with current density in three cycles. The first cycle is with powder specimens which sinter. Cycles 2 and 3 are on the samples that have been sintered to full density in cycle one. (A) The powder sample shows a high resistance initially arising from particle–particle interfaces. (B) The resistance change in Cycles 1 and 2 are shown at a higher resolution resistivity scale. The literature value of the temperature dependent resistance of W is included .

3.2 | Measurement of resistivity

The specific resistivity of tungsten was measured by the four point method. The results are shown in Figure 4. The experiments were done not only in the initial sintering cycle (Cycle 1) with the powder-pressed dog bone sample, but again after sintering, which was repeated in Cycles 2 and 3. The resistance shows a transient peak (at 1200 μΩ) in the first cycle presumably from the abrupt breakdown of the resistance at particle interfaces, which was likely due to thin oxide films. The decline in resistance past the peak is attributed to the sintering of pores. Once sintered the resistance is seen to rise with temperature. The sample is fully sintered after the first cycle. This sintered specimen when flashed again in Cycles 2 and 3 shows consistent behavior. However, the shape of the curve is different and also higher relative to the literature data.[18] These differences are attributed to flash-generated defects such as vacancy–interstitial pairs.

3.3 | Measurement of temperature and electroluminescence

The temperature was measured with the pyrometer. The literature value for the emissivity of tungsten is 0.35. The pyrometer was calibrated with respect to the furnace temperature by focusing it on an tungsten specimen (without current) placed within the furnace. The pyrometer measurements, with the emissivity set at three values, 0.25, 0.30, and 0.35, were compared. Programing the pyrometer with a lower emissivity yielded a slightly higher temperature. The spread between the high and the low emissivity ranged from 10 to 25°C. Accordingly, the specimen temperature was about 50°C higher than the furnace temperature, presumably because the furnace thermocouple was placed near the outer body of the furnace. Therefore, the temperature measured with the pyrometer is assigned an error bar of ~50°C.

The temperature of the specimen was measured continuously during the process of flash sintering. The results for furnace-OFF and furnace-ON experiments are shown together in Figure 5A. A comparison between them is highlighted by the following features:

(i) The first inflexion in the curves for both cases occurs at approximately ~7 A mm^{-2}, after which the temperature remains at a slightly elevated plateau, even though electrical energy is being injected at a steadily increasing rate. It seems reasonable to infer that the energy imparted by the increasing current density without an increase in the specimen is used up in the endothermic reaction of defect formation.
(ii) The onset of electroluminescence, given in Figure 5B, also starts at this inflexion (at ~7 A mm^{-2}).
(iii) A third feature of Figure 5A is the temperature for the onset of full sintering. The current density at sintering is shown in Figures 3 and 4. It occurs at 6–8 A mm^{-2} for the furnace-ON condition, and at 20 A mm^{-2} for the furnace-OFF condition. However, in both cases sintering onsets occur at ~1000°C.

The above discussion leads to a pattern for the progression of flash sintering in metals, which appears to occur in three steps: At first there is an incubation time, that is followed by the temperature rising toward a plateau,

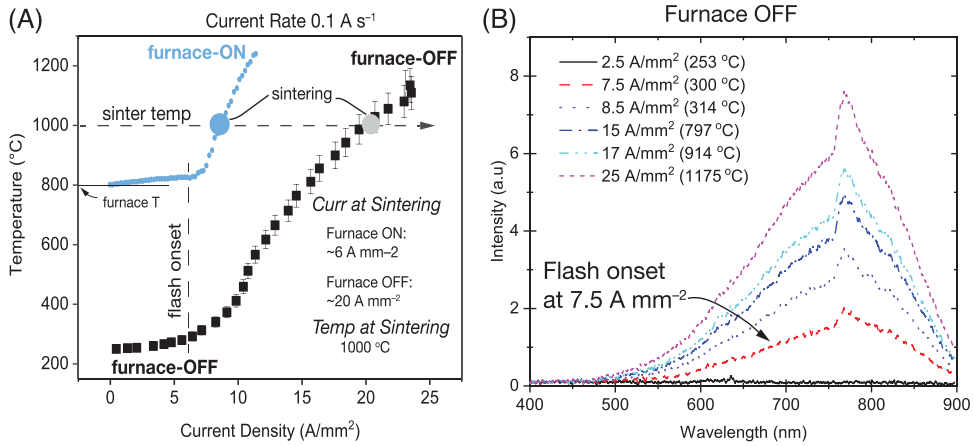

FIGURE 5 (A) The progression in temperature with current density for furnace-ON and OFF experiments. The transition to flash after an incubation regime occurs at the same current density in both ON and OFF experiments; however, the onset of sintering occurs at different current densities but at the same temperature. (B) The electroluminescence spectra with increasing current density. Note that the sample begins to luminesce at the "flash onset" as shown in the left figure.

and finally an upward trajectory of the temperature when the sample sinters. The first transition, which occurs near 7 A mm^{-2}, is accompanied by electroluminescence. During the plateau defects continue to form, consistent with an increasing intensity of luminescence, seen in Figure 5B. At some point, it seems that the defect density reaches a saturation point and the temperature begins to rise with the current density. Why sintering occurs at this saturation point is not clear. Also not understood is why sintering occurs at the same temperature with or without the furnace (~1000°C). The current density at sintering is lower with the furnace as less current is needed to reach this critical temperature.

3.4 | Calorimetry: endothermic enthalpy

In our experience in flash experiments with both metals and ceramics, we have discovered a discrepancy between the input electrical energy and the energy lost to radiation, convection, and specific heat.[14,13] This difference, the energy deficit, is attributed to the endothermic generation of defects, as described by the analysis described below.

We write the equation for the energy deficit, $\Delta H^*(t)$, in Joules, as

$$\Delta H^*(t) = \int_0^t (W(t) - W^*(t))\, dt \tag{3}$$

where $W(t)$ is the electrical work expended (in W) into the sample, and $W^*(t)$ is the energy lost to radiation, convection, and specific heat. $W(t)$ is equal to the product of the voltage and the current.

The energy loss is the sum of three terms: black body radiation (BBR), convection loss, and the energy stored as specific heat:

$$W^*(t) = W^*_{BBR}(t) + W^*_{conv}(t) + W^*_{spht}(t) \tag{4}$$

Each of the above terms are given by the following expressions:

$$W^*_{BBR}(t) = \in_m S\sigma(T_K^4 - 298^4), \tag{5a}$$

$$W^*_{conv}(t) = hS(T_K - 298), \tag{5b}$$

$$W^*_{spht}(t) = mC_p \frac{dT_K}{dy} \tag{5c}$$

Note that the terms in Equation (5) are in units of W, that is, J s^{-1}. Here, S is the surface area of the specimen, $\in_m$ is the emissivity (equals to 0.35), and σ is the Stefan–Boltzmann's constant (5.6704×10^{-8} W m^{-2} K^{-4}). The ambient temperature of 298 K since the experiment was carried out without the furnace. m is the mass of the specimen (0.000326 kg), and the specific heat, C_p = 133 J $(kg\,K)^{-1}$. T_K is the specimen temperature in Kelvin measured with the pyrometer. Substituting Equations (4) and (5) into (3) gives the estimate of the energy deficit in Joules after the right hand side in Equation (4) is integrated with respect to time.

The value for h, the convective heat transfer coefficient in Equation (5) needs further attention. Its value in air can range from 10 to 100 W m^{-2} K^{-1}. It varies with the chemistry and morphology of the surface, the relative velocity of gas at the interface, and the heat carrying capacity of

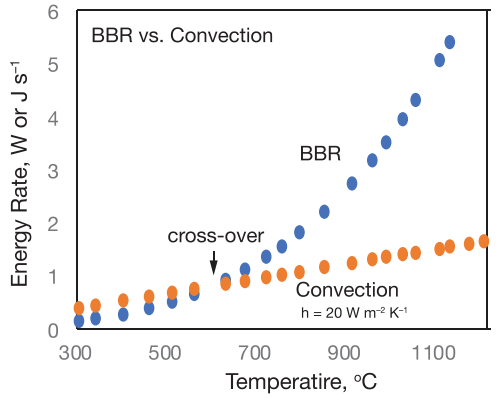

FIGURE 6 Plots of energy loss from black body radiation (BBR) and from convection. The latter depends on the heat transfer coefficient h, which is adjusted, in the present case to 20 W m^{-2} K^{-1}, so that the crossover occurs near 600°C.

the gas, which depends on its pressure and specific heat. For example, Ar has a much lower heat capacity than N_2; therefore, in Ar (used in present experiments) the heat transfer coefficient will be lower than in air.

The convective loss increases linearly with T, whereas BBR increases as T.[4] Therefore, convection dominates at low temperatures but crosses over to BBR at higher temperature. The value for h was assigned by assigning the generally accepted crossover temperature to be about 600°C. It is when the emission color is of mildly red heat, nominally considered the point where the loss transitions from convection to BBR. Such a plot for our data is given in Figure 6, which shows that the transition occurs near 600°C when $h = 20$ W m^{-2} K^{-1}.

The next step is to reduce ΔH^* in Equation (3) to a molar quantity, which is done by first by calculating the number of moles of tungsten in the specimen, as given by

$$N_W = \frac{V_{specimen}}{V_{molar}} \tag{6}$$

Therefore, the enthalpy in Equation (3) as a molar quantity is given by

$$\Delta H^*_{mol} = \frac{\Delta H^*}{N_W} \tag{7}$$

The mole fraction of defects formed in the specimen is obtained by dividing Equation (7) by the energy of formation of the defects,

$$x_F = \frac{1}{E_F}\frac{\Delta H^*}{N_W} \tag{8}$$

where E_F is the formation energy of defects in units of J mol^{-1}.

The following method was used to calculate the results given by Equations (7) and (8). The experimental inputs were the temperature (measured with the pyrometer) and the electrical input power, both as a function of time. The temperature was translated into the parameters on the left hand side of Equation (5); watts were converted into Joules by integrating with time. The Joules stored as specific heat were added to the sum of the BBR and convection to obtain the total energy loss. The input energy was calculated from the integrating the input power with respect to time. The difference between the input and the energy loss gave the magnitude of ΔH^* which was inserted into Equation (8) to obtain the mol fraction of Frenkel defects. The data and the results from the above analysis are given in Tables 1 and 2.

Plots for the energy deficit in kJ mol^{-1} and the corresponding mol fraction of Frenkels pairs are shown in Figure 7. It is rather remarkable that the defect concentration reaches as high as 26% mol fraction. The value calculated from thermal equilibrium is many orders of magnitude smaller. We have checked our experiments and our analysis to be sure. These numbers are perhaps okay since we measure a volume expansion of >5% during flash: Interstitial vacancy pairs carry a small volume expansion—and it is possible that a very large number of them may be needed to explain such a large volume expansion. The defect generation also appears to be different for nickel: as reported in a subsequent manuscript we report a lower value for the mol fraction of Frenkel pairs—about 3%, though that is still very large compared to the thermal equilibrium calculation.

The large mole fraction of defects reflects a new paradigm in the "flash-ecosystem," which is emerging as a far from equilibrium phenomenon, which with chemical reactions and mass transport by diffusion occur at astronomical rates.

3.5 | Molecular dynamics

The athermal generation of Frenkel pairs has been thought to arise from nonlinear lattice vibrations, which are possible only if the phonon wavelengths are less than or equal to the lattice parameter, that is at the edge of the Brillouin Zone, with the practical implication that the defects can form only above the Debye temperature. This hypothesis was validated by experiments where three oxides were shown to flash only when above Debye.[19,20] Molecular dynamics simulations with single crystals aluminum also proved that Frenkel pairs could be generated by proliferation of such phonons.[21] These results are described in Figure 8.

TABLE 1 Analysis of time, temperature, electrical power input for obtaining the energy deficit, and from that the mole fraction of Frenkel defects.

Specimen volume = 20.7 mm^3											
Surface area = 7 mm^2											
C_p = 133 J kg^{-1} K^{-1}											
Frenkel formation energy = 1610 kJ mol^{-1}											
h = 20 W m^{-2} K^{-1}											
s = 5.67 × 10^{-8} W m^{-2} K^{-4}											
Emissivity = 0.35											
Molar volume = 9.5 cm^3 mol^{-1}											
C1	**C2**	**C3**	**C4**	**C5**	**C6**	**C7**	**C8**	**C9**	**C10**	**C11**	**C12**
Time (s)	**Pyro Temp (°C)**	**Watts**	**BBR (W)**	**BBR total (J)**	**Convec (W)**	**Convec total (J)**	**Spec total (J)**	**Total IN (J)**	**total loss (J)**	**Deficit (kJ mol^{-1})**	**Frenkel mol fraction**
217	341	1.81	0.2	26	0.44	77	14	229	117	52	0.032
234	403	2.07	0.3	5	0.53	86	16	265	107	72	0.045
247	460	2.28	0.4	10	0.61	94	19	295	123	79	0.049
256	511	2.47	0.5	14	0.68	100	21	317	136	83	0.052
269	562	2.72	0.7	23	0.75	110	23	353	157	90	0.056
289	632	3.17	0.9	41	0.85	127	26	415	195	101	0.063
306	674	3.56	1.1	61	0.91	143	28	477	231	113	0.070
331	722	4.11	1.3	94	0.97	166	30	578	290	132	0.082
346	757	4.40	1.5	117	1.02	182	32	643	330	144	0.089
373	797	5.03	1.8	165	1.08	211	33	779	410	169	0.105
389	852	5.38	2.2	201	1.16	229	36	865	466	183	0.114
418	914	6.24	2.7	282	1.24	266	39	1049	586	212	0.132
438	958	6.84	3.2	344	1.31	292	40	1183	677	232	0.145
462	990	7.62	3.5	431	1.35	325	42	1371	798	263	0.164
492	1026	8.20	3.9	548	1.40	366	43	1613	957	301	0.187
517	1056	8.93	4.3	654	1.44	402	45	1833	1100	336	0.209
546	1109	9.80	5.1	803	1.52	446	47	2122	1296	379	0.236
548	1132	9.81	5.4	816	1.55	450	48	2146	1314	381	0.238
567	1175	10.34	6.1	927	1.61	480	50	2334	1457	402	0.251
590	1209	11.07	6.7	1085	1.66	519	51	2596	1655	432	0.269

Abbreviation: BBR, black body radiation.

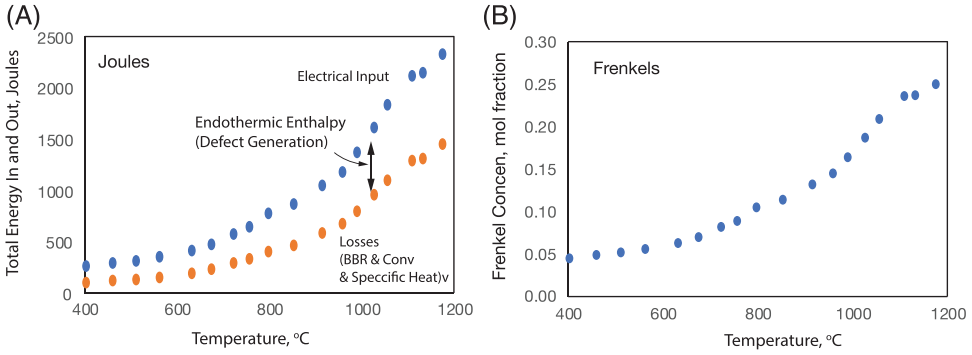

FIGURE 7 (A) The energy deficit calculated from the difference between the input electrical energy and the energy lost to radiation, convection, and specific heat. (B) Estimate of the defect concentrations from the energy deficit and the energy of formation of the Frenkels.

TABLE 2 Column by column explanation of the analysis is given in Table 1.

Column	Description
C1	Time in seconds—the clock starteh when the temperature rose above ~350°C since that is the threshold for accurate measurement with the pyrometer
C2	The temperature measured with the pyrometer
C3	Total electrical power expended in the specimen (product of volts and amperes)
C4	Watts lost to BBR as given by Equation (5a)
C5	Joules lost to BBR obtained from integration of C4
C6	Watts lost to convection as given by Equation (5b)
C7	Joules lost to convection obtained from integration of C6
C8	Joules stored in specific heat (integration of Equation 5c)
C9	Joules input from electrical energy: obtained from integration of C3
C10	Total energy loss = the sum of C5 + C7 + C8 in Joules
C11	The difference between input energy and energy loss in kJ mol^{-1} (from Equations 6 and 7)
C12	The concentration of Frenkel pairs obtained by dividing C11 (kJ mol^{-1}) by the energy of formation of Frenkel's in kJ mol^{-1}

Abbreviation: BBR, black body radiation.

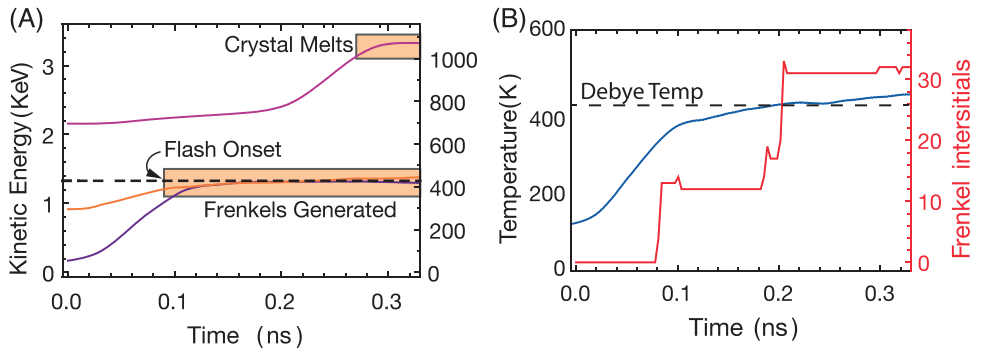

FIGURE 8 (A) Kinetic energy of phonons injected into an aluminum single crystal at first raises the temperature but then plateaus above the Debye temperature, thereafter, as shown in (B) the energy is consumed in the generation of Frenkels, this behavior is similar to the data in Figure 5 where the temperature of the specimen does not increase as the current density is increases, presumably consumed in the endothermic reaction of defect generation.

Figure 8A shows the influence of continuous injection of current density on the change in the temperature of the crystal. The temperature rises up to the Debye temperature but then plateaus as the energy is consumed by the generation of defects as shown in Figure 8B. It is interesting that the Frenkel concentration does not increase smoothly but in abrupt steps.

3.6 | Phenomenological description of flash in metals

The pattern of flash sintering behavior in the present work is similar to experiments of flash sintering of Ni (unpublished). Notably, in Ni and in W, the change in resistance differs significantly from the literature values, most likely reflecting the influence of defects that are generated during the flash process.

As shown in Figure 9 the general features are reflected similarly in the change of resistance as well as the estimate of the Frenkel pairs described in Section 3.4. They consist of an incubation time up to the onset of luminescence, which is followed by a shallow plateau in temperature and generation of defects. Finally, the temperature turns upward and sintering occurs abruptly. Similar behavior was observed in Ni.

Sintering in flash is quite different than conventional sintering. For example, let us compare Ni and W, with melting points of 1455 and 3383°C. Normally, diffusion rates that occur at $0.75T_M$ are needed for sintering within a few hours. Therefore, conventional sintering of tungsten requires much higher temperatures (~2450°C) than nickel

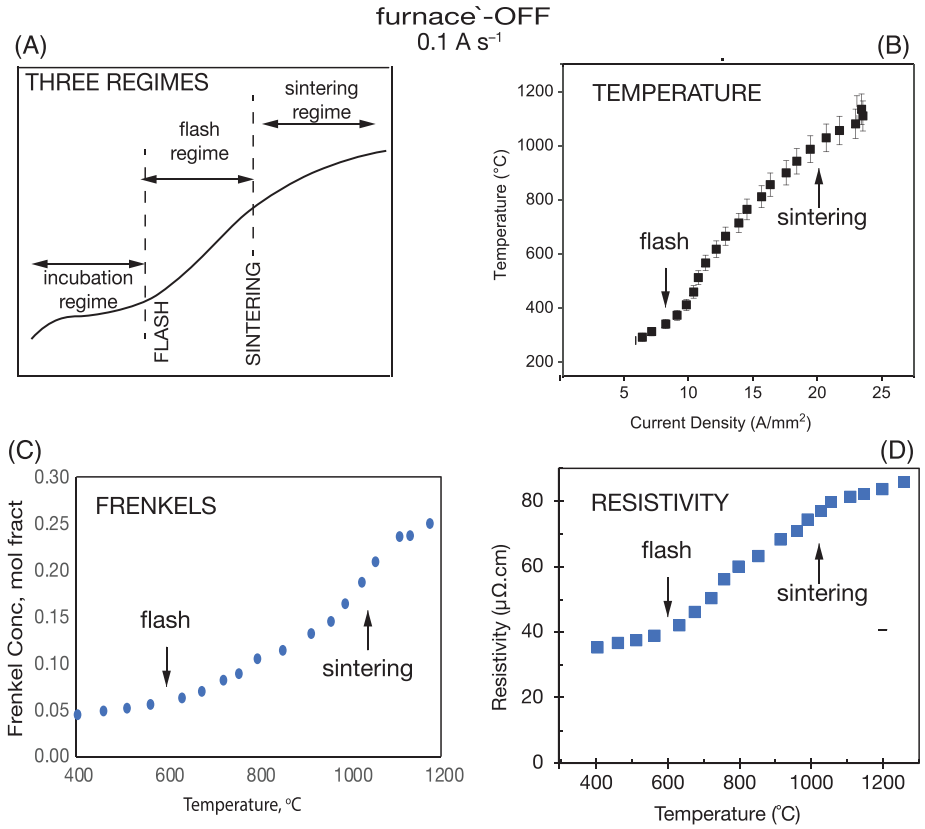

FIGURE 9 (A) The three regimes characterizing the phenomenological behavior in flash sintering of metals; the transitions are prescribed by three regimes: the incubation regime, followed by the flash regime, followed by the sintering to full density. The measurement of (B) temperature, (C) the estimate of defect generation, and (D) the resistivity, consistently show this three-regimes pattern.

(~1023°C). In flash both metals sinter at a temperature of 1000°C (for specimens of similar geometry), at a similar current density of ~20 A mm^{-2}.

4 | MICROSTRUCTURE AND HARDNESS

The microstructure of the specimens was obtained from cut and polished cross sections. The specimens were mounted using Allied QuickCure powder and liquid then cured at room temperature for 5 min. The mounted specimens were polished using a LECO VP-160 machine using polishing papers ranging from 240 to 1 μm. The specimens were then rinsed, dried, and etched using a 30% hydrogen peroxide for 60 s. The etched specimens were immediately rinsed in water.

A Hitachi SU3500 SEM (Colorado Shared Instrumentation in Nanofabrication and Characterization—COSINC) was used to observe the microstructure of the specimens. The micrographs were obtained in the back scattering mode at 15 kV. The micrographs of the unsintered and sintered samples are shown in Figure 10. The grain size in the sintered samples is about three to four times the size of the powder particles, about 12 μm. Therefore, significant grain growth took place during sintering.

Vickers Hardness was measured using the standard ISO 6507-12018 via the Rockwell Hardness tester situated in Idea Forge, University of Colorado Boulder with a diamond indenter. The hardness value was obtained using:

$$H_v = \frac{2F \sin \frac{136^\circ}{2}}{d^2} = 1.854 \frac{F}{d^2} \quad (9)$$

where d is the average diagonal length of the indentation in mm and F is the load in kg.

Twelve measurements were made with 12 kgf and one with 45 kg. The image of the indentation was captured using optical microscope and the diagonal was measured using Fiji software. The H_v for 12 kg ranged from 393 to 596. The measurement with 45 kg gave H_v 438. The average of all these values, 467 is given in Table 3. The data from other methods was obtained from Tan et al.[22] The flash sintered specimens gave hardness values that are quite comparable with literature values.

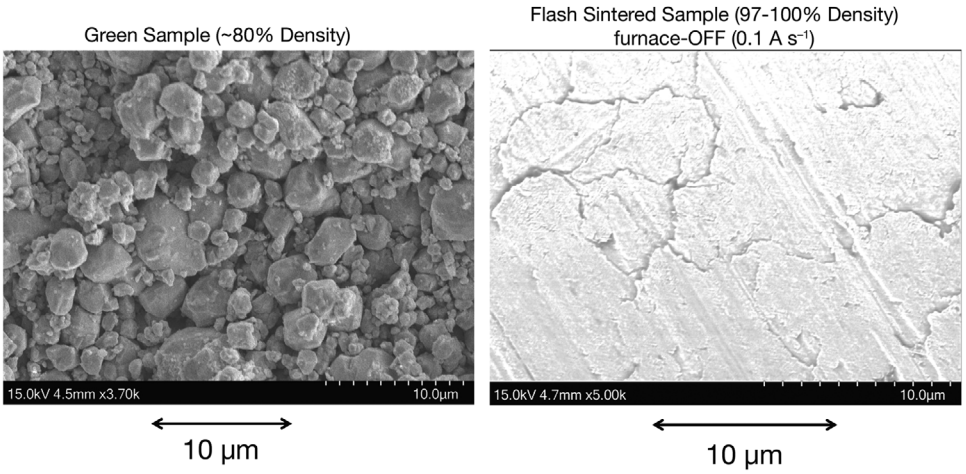

FIGURE 10 SEM micrograph of polished and etched cross section of a flash sintered specimen. Nearly full density was achieved. The grain size was approximately 10 mm, somewhat similar to the particle size in the green sample.

TABLE 3 A comparison of the hardness values for the current specimens and those processing in different ways from the literature.[22]

Fabrication method	Relative density (%)	H_v
Selective laser melting	97—98	445—467
Chemical vapor deposition	≤99.79	419
Powder metallurgy	≤98	320—400
Hot Isotactic pressing	≤98.20	344
Spark plasma sintering	≤96.30	372
Flash sintering	>98	467

5 | DISCUSSION

The present work is not only the first conclusive example of the application of flash to metals, it also highlights the remarkable sintering of a highly refractory metal (tungsten incandescent lamps operate above 2700°C). In other work, in progress, we show that flash sintering of a nominal metal like nickel, occurs at about the same temperature as tungsten. Thus, conventional views that sintering is related to the concepts of solid-state diffusion, which scales with the melting temperature, no longer apply. Flash is a new phenomenon where mass transport occurs by a different science.

The earliest evidence of possible flash in metals was experimented by McWilliams et al.[23] with aluminum powder, where an abrupt increase in densification was attributed to the breakdown of the oxide films. More recently Mazo et al.[24] have shown sintering of tungsten carbide with electrical activation. Graphitization of amorphous carbon under flash was demonstrated by Ingraci and Raj.[25]

Although ceramics require furnace heating to initiate flash sintering, metals do not. They can be sintered without a furnace by direct injection of current. Nevertheless, we have presented results with and without a furnace. Interestingly, in both cases, sintering occurs when the specimen reaches 1000°C. The current density to reach this temperature is of course lower (7.5 A mm^{-2}) with furnace heating, than without the furnace (20 A mm^{-2}).

The measurements of the change in specific resistivity with temperature differ from those reported in literature. Although nominally the resistance increases monotonically with temperature, the in-operando flash data show inflexions. At first the resistance exhibits a shallow plateau, rising slowly with temperature. It transitions into rising value with a higher slope and then bends over to a lower slope similar to the literature values.

This unusual shape of the resistance versus temperature curve may contain information on the generation of defects. Indeed the estimate of defect concentrations from energy deficit calculations, shown in Figure 7B, shows a shape that is similar to shape of the resistance curve. Such concentrations of Frenkel defects are many orders of magnitude greater than expected from thermal equilibrium.

The result in Figure 3, where the sintering strain is shown to be independent of the current rate is intriguing. We rationalize this unusual result by recognizing that the rate of mass transport by diffusion depends on the product of the defect concentration and the mobility of defects. If the defect concentration is very large then it may weaken the influence of mobility on the rate of mass transport. As the defect concentration depends on the current density, it can be postulated that sintering will also predominantly depend on the current density.

It is of note that sintering of tungsten powder with electrical currents was practiced more than a century ago[26] in the quest of fabricating fine ductile tungsten wire for incandescent lamps. Eventually this process succeeded in trapping bubbles of potassium, which having a high vapor pressure, could be retained only if the sintering was accomplished in split seconds. These bubbles stretched out into strings during hot extrusion. Thus, they restrained grain growth in the transverse direction of the wire, yielding pseudo-single crystal structure that is highly creep resistant and for nearly a century was used as the heating element in incandescent lamps[27]

6 | CONCLUSIONS

The present experiments on tungsten and ongoing work in our laboratory are showing that metals can be flash sintered just like ceramics. Metals are unique in that they can be sintered without a furnace by injecting current and increasing it at a constant rate. However, sintering depends only on the instantaneous value of the current density: It is independent of the current rate.

In conventional sintering temperature and time control the rate of sintering require a furnace. In flash sintering consolidation is achieved, without a furnace, by injecting "energy" directly into the specimen. Thus, electrical energy is immediately transferred into the chemical work required for sintering. Thus, flash carries a huge benefit in energy efficiency. Simple estimates show that flash uses <1% of the energy used in conventional processing.

The energy efficiency of flash sintering can be compared to the electrification of cars where electrical power is injected directly into motors that drive the wheels, thereby sidestepping inefficient internal combustion engines. Here, electrical energy is injected directly into the workpiece for doing the work of sintering, obviating the need for large furnaces that waste heat. The electrification of manufacturing of metals and ceramics suddenly seems a plausible.

The present experiments are quite different from electro-discharge-sintering where a large quantum of energy stored in a capacitor is dumped into the metal in few tens of milliseconds to achieve sintering. Here, sintering is controlled by a measured rate of current injection, which can stretch the sintering time from a few seconds to several minutes.

Finally, we see an application of flash sintering of metals in the manner shown here in additive manufacturing for producing ready to use, dense workpieces.

ACKNOWLEDGMENTS

The authors greatly acknowledge Alan Weimer's research group members at the University of Colorado Boulder for their contributions during group meetings. This work was supported by a grant from NASA, ESI Program under grant number 80NSSC21K0225. We are grateful to Dr. Jhonathan Rosales, at NASA, for his guidance and enthusiastic support during the course of this research. RR owes gratitude to Dr. G. W. King at Westinghouse Electric in Broomfield where he was shown that a powder ingot of W anchored at one end to a high current electrode with the other end immersed in liquid mercury that sintered almost instantaneously with a bright glow when the current was energized. Such observations long embedded in memory stimulate new fundamental discoveries later in life.

ORCID

Alan W. Weimer https://orcid.org/0000-0002-2471-349X
Rishi Raj https://orcid.org/0000-0001-8556-9797

REFERENCES

1. Katz JD. Microwave sintering of ceramics. Annu Rev Mater Sci. 1992;22(1):153–70. https://doi.org/10.1146/annurev.ms.22.080192.001101
2. Anselmi-Tamburini U, Gennari S, Garay JE, Munir ZA. Fundamental investigations on the spark plasma sintering/synthesis process: II. Modeling of current and temperature distributions. Mater Sci Eng: A. 2005;394(1):139–48. https://doi.org/10.1016/j.msea.2004.11.019
3. Grasso S, Saunders T, Porwal H, Milsom B, Tudball A, Reece M. Flash spark plasma sintering (FSPS) of α and β SiC. J Am Ceram Soc. 2016;99(5):1534–43. https://doi.org/10.1111/jace.14158
4. Cologna M, Rashkova B, Raj R. Flash sintering of nanograin zirconia in< 5 s at 850 C. J Am Ceram Soc. 2010;93(11):3556–59.
5. Gil-González E, Pérez-Maqueda LA, Sánchez-Jiménez PE, Perejón A. Flash sintering research perspective: a bibliometric analysis. Materials. 2022;15(2):416. https://doi.org/10.3390/ma15020416
6. Wan J, Duan R-G, Mukherjee AK. Spark plasma sintering of silicon nitride/silicon carbide nanocomposites with reduced additive amounts. Scr Mater. 2005;53(6):663–67.
7. Yu M, Grasso S, Mckinnon R, Saunders T, Reece MJ. Review of flash sintering: materials, mechanisms and modelling. Adv Appl Ceram. 2017;116(1):24–60. https://doi.org/10.1080/17436753.2016.1251051
8. Kermani M, Hu C, Grasso S. From pit fire to ultrafast high-temperature sintering (UHS): a review on ultrarapid consolidation. Ceram Int. 2022;49(3):4017–29 https://doi.org/10.1016/j.ceramint.2022.11.091
9. Guo J, Guo H, Baker AL, Lanagan MT, Kupp ER, Messing GL, et al. Cold sintering: a paradigm shift for processing and integration of ceramics. Angew Chem Int Ed. 2016;55(38):11457–61. https://doi.org/10.1002/anie.201605443
10. Raj R, Wolf DE, Yamada CN, Jha SK, Lebrun J-M. On the confluence of ultrafast heating rate sintering and flash sintering phenomena. J Am Ceram. 2023;106(7):3983–98.
11. Terauds K, Lebrun J-M, Lee H-H, Jeon T-Y, Lee S-H, Je JH, et al. Electroluminescence and the measurement of temperature during stage III of flash sintering experiments. J Eur Ceram Soc. 2015;35(11):3195–99. https://doi.org/10.1016/j.jeurceramsoc.2015.03.040

12. Lebrun J-M, Raj R. A first report of photoemission in experiments related to flash sintering. J Am Ceram Soc. 2014;97(8):2427–30. https://doi.org/10.1111/jace.13130
13. Mishra TP, Neto RRI, Raj R, Guillon O, Bram M. Current-rate flash sintering of gadolinium doped ceria: microstructure and defect generation. Acta Mater. 2020;189:145–53. https://doi.org/10.1016/j.actamat.2020.02.036
14. Kumar MK P, Yadav D, Lebrun J, Raj R. Flash sintering with current rate: a different approach. J Am Ceram Soc. 2019;102(2):823–35.
15. Yurlova MS, Demenyuk VD, Lebedeva LYU, Dudina DV, Grigoryev EG, Olevsky EA. Electric pulse consolidation: an alternative to spark plasma sintering. J Mater Sci. 2014;49(3):952–85. https://doi.org/10.1007/s10853-013-7805-8
16. Hiernaut J-P, Sakuma F, Ronchi C. Determination of the melting point and the emissivity of refractory metals with a six-wavelength pyrometer. High Temp High Press (Print). 1989;21(2):139–48.
17. Raj R. Separation of cavitation-strain and creep-strain during deformation. J Am Ceram. 1982;65(3):C-46.
18. Jones HA. A temperature scale for tungsten. Phys Rev. 1926;28(1):202–7. https://doi.org/10.1103/PhysRev.28.202
19. Yadav D, Raj R. Two unique measurements related to flash experiments with yttria-stabilized zirconia. J Am Ceram Soc. 2017;100(12):5374–78. https://doi.org/10.1111/jace.15114
20. Mishra TP, Avila V, Neto RRI, Bram M, Guillon O, Raj R. On the role of Debye temperature in the onset of flash in three oxides. Scr Mater. 2019;170:81–84. https://doi.org/10.1016/j.scriptamat.2019.05.030
21. Jongmanns M, Raj R, Wolf DE. Generation of Frenkel defects above the Debye temperature by proliferation of phonons near the Brillouin zone edge. New J Phys. 2018;20(9):093013. https://doi.org/10.1088/1367-2630/aadd5a
22. Tan C, Zhou K, Ma W, Attard B, Zhang P, Kuang T. Selective laser melting of high-performance pure tungsten: parameter design, densification behavior and mechanical properties. Sci Technol Adv Mater. 2018;19(1):370–80. https://doi.org/10.1080/14686996.2018.1455154
23. McWilliams B, Yu J, Kellogg F, Kilczewski S. Enhanced sintering kinetics in aluminum alloy powder consolidated using DC electric fields. Metall Mat Trans A. 2017;48(2):919–29. https://doi.org/10.1007/s11661-016-3861-4
24. Mazo I, Molinari A, Sglavo VM. Electrical resistance flash sintering of tungsten carbide. Mater Des. 2022;213:110330. https://doi.org/10.1016/j.matdes.2021.110330
25. Ingraci Neto RR, Raj R. The flash effect in electronic conductors: the case of amorphous carbon fibers. Scr Mater. 2020;179:20–24. https://doi.org/10.1016/j.scriptamat.2020.01.003
26. Coolidge, W.D. Tungsten and method of making the same for use as filaments of incandescent electric AMPS and for other purposes. US1082933A. 1913.
27. Raj R, King G. Life prediction of tungsten filaments in incandescent lamps. Metall Trans A. 1978;9(7):941–46.

How to cite this article: Bamidele E, Jalali SIA, Weimer AW, Raj R. Flash sintering of tungsten at room temperature (without a furnace) in <1 min by injection of electrical currents at different rates. J Am Ceram Soc. 2024;107:817–829. https://doi.org/10.1111/jace.19532